Improving Single Shot Acquisitions with Fast Rotary Nonlinear Spatial Encoding

Haifeng Wang[1], Leo Tam[1], R. Todd Constable[1], and Gigi Galiana[1]
[1]*Department of Diagnostic Radiology, Yale University, New Haven, CT, United States*

TARGET AUDIENCE: Researchers interested in accelerated imaging and imaging with nonlinear gradients

PURPOSE: Spatial encoding with nonlinear magnetic fields has been studied as a means to encode images acquired with multichannel receiver coils using fewer echoes. This has been the primary motivation for O-Space [1] and Null Space [2] imaging, and has also been explored with PatLoc [3], 4D-RIO[4], and others. These approaches may overcome physiological limitations of the conventional linear gradient system to accelerate the data acquisition in the presence of multiple receiver coils [5]. Previous nonlinear gradient encoding works [6-9] have also explored single shot trajectories in nonlinear magnetic fields. Like Ref. 9, this work uses time varying nonlinear gradients and focuses on compressible waveforms. In this work, we present a novel scheme of fast rotary nonlinear spatial encoding, named as FRONSAC imaging. The linear gradients are applied on the three standard linear encoding fields, and the rotary gradients, or sinusoidal gradient moments, are applied on two second-order encoding fields. Images are reconstructed by Kaczmarz algorithm [10]. The simulations show a low amplitude fast rotating second-order field seems to greatly aid many highly under-sampled linear trajectories. And the results illustrate that the proposed scheme can improve image quality in accelerated data acquisitions.

METHODS: Neglecting relaxation effects, the magnetic resonance signal $s_j$from the j-th RF channel, $s_j = \int M(\boldsymbol{X})C_j(\boldsymbol{X})e^{i\Phi(\boldsymbol{X},t)}d\boldsymbol{X}$, where $M(\boldsymbol{X})$ is the magnetization at position $\boldsymbol{X}$, $C_j(\boldsymbol{X})$ is the sensitivity of coil j , and $\Phi(\boldsymbol{X},t)$ is the spatially dependent encoding phase, which can be decomposed as $\Phi(\boldsymbol{X},t) = \boldsymbol{\kappa}^T(t)\Psi(\boldsymbol{X})$. $\boldsymbol{\kappa}(t)$ is the vector of gradient moments, and $\Psi(\boldsymbol{X})$ represents the gradient encoding fields at position $\boldsymbol{X} = (x,y,z)$, which defines a position in three dimensions. Here, the gradient moments $\boldsymbol{\kappa}(t)$ and the gradient waveforms $\boldsymbol{g}(t)$ should satisfy the following equation: $\boldsymbol{\kappa}(t) = \gamma\int_0^t \boldsymbol{g}(\tau)d\tau$. This work is based on the currently existing hardware of three traditional standard linear encoding fields from scanners and two quadrupolar encoding fields generated from a custom-built gradient insert. Thus, at the hardware level, this imaging system would be controlled by five gradient waveforms $\boldsymbol{g}(t) = \left[g_x(t), g_y(t), g_z(t), g_{xy}(t), g_{x^2-y^2}(t)\right]^T$, where $\boldsymbol{g}(t)$ can be written as $\boldsymbol{g}(t) = [\boldsymbol{g}_L(t),\ \boldsymbol{g}_{NL}(t)]^T$. Thus, $\boldsymbol{g}_L(t)$ describes the linear gradients $\boldsymbol{g}_L(t) = \left[g_x(t), g_y(t), g_z(t)\right]^T$, while $\boldsymbol{g}_{NL}(t)$ describes two second-order nonlinear gradients $\boldsymbol{g}_{NL}(t) = \left[g_{xy}(t), g_{x^2-y^2}(t)\right]^T$. Because of safety and hardware limitations, the additional nonlinear gradients must still obey constraints on the maximum gradient amplitude $\boldsymbol{g}_{max}$ and the gradient slew rate $\boldsymbol{s}_{max}$ for the total linear and nonlinear gradients, i.e. $|\boldsymbol{g}(t)| \le \boldsymbol{g}_{max}$ and $|\partial\boldsymbol{g}(t)/\partial t| \le \boldsymbol{s}_{max}$. In each of our simulations, $\boldsymbol{g}_L(t)$ has the shape of standard gradient waveforms, such as, EPI [11], Spiral [12, 13], or Rosette [14]. $\boldsymbol{g}_{NL}(t)$ contains fast rotary gradient waveforms with low amplitudes and fast oscillations, as seen as Fig. 1. More specifically, $\boldsymbol{g}_{NL}(t) = [A_{NL}sin(\omega_0 t), A_{NL}cos(\omega_0 t)]^T$, ω_0 is the angle rate and A_{NL} is the maximum amplitude along 2 second-order gradients. To reconstruct the highly under-sampled dataset, we apply the Kaczmarz algorithm. As described in reference [15], nonlinear gradient moment spreads the sampling function in k-space, such that each collected data-point reflects a weighted sum of k-space points. However, while this sampling scheme is efficient in that it acquires many k-space points at once, it can sometimes be difficult to solve for the individual points comprising the sampled k-space, leading to artifacts. With our proposed method, the nonlinear gradient moment causes a small square of k-space to be sampled with each data-point, but as the linear gradient moment translates the square through k-space, the sinusoidal oscillation causes this square to rapidly rotate, as seen in Fig.2. Thus, acquiring various orientations of the sampling function may allow us to more effectively acquire a broad swath of k-space points while retaining the independent information needed to distinguish the individual points being sampled.

RESULTS: We studied three traditional types of highly under-sampled single shot trajectories, EPI, Spiral and Rosette, with the proposed method like that shown in Fig. 3. These would theoretically allow us to acquire the all data in 4.25ms without exceeding the mean threshold for peripheral nerve stimulation discomfort (55/s) over a 20cm field of view. This acquisition scheme would imply a dwell time of approximately 1μs. Here, two simulations including Gaussian noise and dephasing effects are shown in Fig. 4. Readout sampled total 4096 points, encoding was simulated in MATLAB at a 64^2 matrix size and white noise was added with amplitude 1% of the mean of the simulated image intensity. The simulations used experimental receiver coil profiles from an 8 channel coil. For EPI, Spiral and Rosette, $\omega_0/2\pi$ are all 11kHz; A_{NL} are all 300Hz/cm^2. The results show the proposed methods of Rosette, Spiral and EPI decreased artifacts and remarkably improved resolutions in single shot acquisitions. Further simulations show that the proposed methods also can easily be generalized to multiple-shot acquisitions.

DISCUSSION AND CONCLUSION: All results illustrate that the proposed schemes presented here distinctly eliminate aliasing artifacts allowing faster imaging speeds. Though single shot acquisitions require high performance gradients to allow rapid switching of the gradients, the proposed method has the advantages of an overall shorter scan time than conventional methods.

REFERENCES: **1**. Stockmann et al. MRM. 64(2): 447-456, 2010; **2**. Tam et al. MRM. 69(4): 1166-1175, 2012; **3**. Hennig et al. MAGMA. 21(1-2): 5-14, 2008; **4**. Gallichan et al. MAGMA. 25(6): 419-431, 2012; **5**. Galiana et al. CMR Part A 40A(5): 253-267, 2012; **6**. Layton et al. MRM. 70(3): 684-696, 2013; **7**. Gallichan et al. ISMRM. 0292, 2012; **8**. Littin et al. ISMRM. 2379, 2013; **9**. Galiana et al. ISMRM. 0013, 2013; **10**. Herman et al. J. Theo. Biol. 42: 1-32, 1973; **11**. Mansfield et al. JMR. 29: 355-373, 1978; **12**. Ahn et al. TMI. 5(1): 2-7, 1986; **13**. Meyer et al. MRM. 28: 202-213, 1992; **14**. Noll, TMI. 16(4): 372-377, 1997; **15**. Stockmann et al. MRM. 69(2): 444-455, 2013.

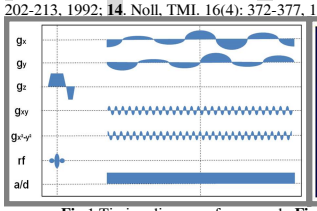

Fig.1 Timing diagram of proposed pulse sequence

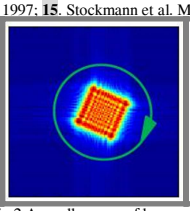

Fig.2 A small square of k-space points with fast oscillating (green arrow)

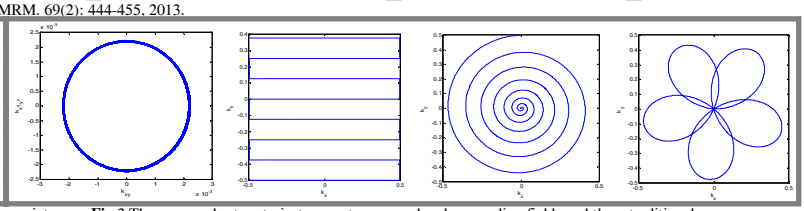

Fig.3 The proposed rotary trajectory on two second-order encoding fields and three traditional types of single shot trajectories, EPI, Spiral and Rosette, on three linear encoding fields

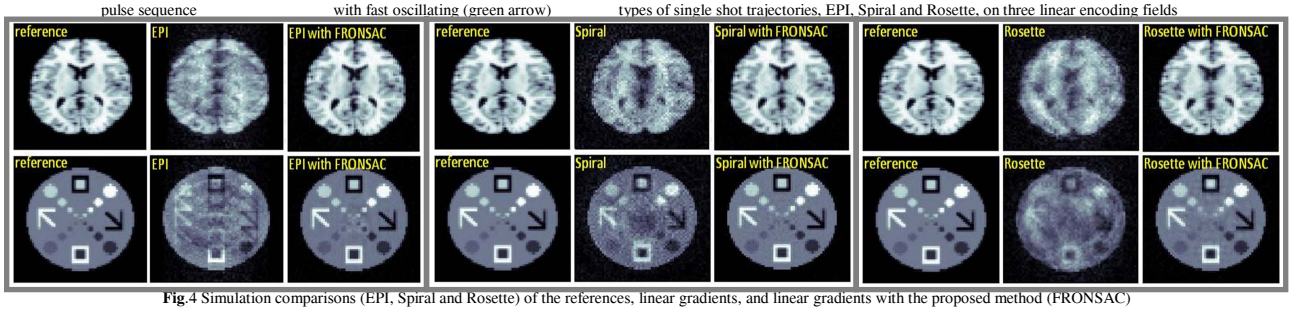

Fig.4 Simulation comparisons (EPI, Spiral and Rosette) of the references, linear gradients, and linear gradients with the proposed method (FRONSAC)